Numerical and renormalization group analysis of the phase diagram of a stochastic cubic autocatalytic reaction-diffusion system

Alberto P. Muñuzuri [1,2,3] Jean-Sébastien Gagnon [1,4] and Juan Pérez-Mercader [1,5]

[1]*Department of Earth and Planetary Sciences, Harvard University, Cambridge, Massachusetts 02138-1204, USA*
[2]*Group of Nonlinear Physics, University of Santiago de Compostela, 15706 Santiago de Compostela, Spain*
[3]*Galician Center for Mathematical Research and Technology (CITMAga), 15782 Santiago de Compostela, Spain*
[4]*Department of Physics, Norwich University, Northfield, Vermont 05663, USA*
[5]*Santa Fe Institute, Santa Fe, New Mexico 87501, USA*

(Received 8 November 2022; accepted 14 March 2023; published 30 March 2023)

The renormalization group is a set of tools that can be used to incorporate the effect of fluctuations in a dynamical system as a rescaling of the system's parameters. Here, we apply the renormalization group to a pattern-forming stochastic cubic autocatalytic reaction-diffusion model and compare its predictions with numerical simulations. Our results demonstrate a good agreement within the range of validity of the theory and show that external noise can be used as a control parameter in such systems.

DOI: 10.1103/PhysRevE.107.034213

I. INTRODUCTION

Complex spatiotemporal patterns observed in nature [1,2] have been the object of intensive research and fascination for a long time. Some attempts to model the existence of these patterns have been tried within different contexts. One of the most promising classes of theoretical models that preserves the basic properties of such patterns are those containing diffusion and cubic autocatalytic reaction terms. This class of models has been exhaustively studied both theoretically and numerically in the past [3–6] because of its simplicity and its capability to exhibit numerous naturelike behaviors.

Such models are considered a paradigm for pattern formation. Some of these patterns are related to the ability of those systems to organize into stable stationary nonhomogeneous structures called Turing structures. First theoretically proposed by Turing [7], and eventually found experimentally [8], they are viewed as a possible explanation of morphogenesis in natural systems. Some other patterns are related to the existence of oscillatory behaviors and wave instabilities (Hopf instabilities) [1,2,9]. This type of nonlinear nonconservative waves (also called autowaves) are indeed ubiquitous in nature and are present in important systems ranging from cardiac cells [10], cultures of mold discoidelium discoideum [11], nerve pulse propagation, and chemical reactions such as the Belousov-Zhabotinsky reaction [12].

Realistically, chemical and biological systems are constantly subjected to variations in their environment. Examples include variations in temperature and fluctuations of active transport of molecules through cell membranes [13]. Similarly, externally tunable noise can be used to influence (and even control) the behavior of chemical or biological systems. For instance, it has been shown that external mechanical noise (shaking vs stirring) can change the output of chemical replicator reactions [14], and that fluctuating illumination can induce coherence resonance in the Belousov-Zhabotinsky reaction [15–17]. Noise (either internal or external) have been shown to influence the formation of certain patterns in reaction-diffusion systems [18–20]. The Selkov-Gray-Scott model with diffusion, called the CARD (cubic autocatalytic reaction-diffusion) model below, has a particularly rich phenomenology in terms of patterns (spiral, stripes, and spots), and has been studied extensively in the presence of noise [21–25], although other models have been studied as well (e.g., Brusselator [26–28], light-sensitive Belousov-Zhabotinsky reaction [29], CDIMA reaction [30,31], and epidemic model [32]). Numerous techniques have been devised to study reaction-diffusion systems analytically [33,34] subjected to various types of noise (e.g., colored noise [35,49] and dichotomous noise [30]). Given the potential of reaction-diffusion systems to model realistic chemical and biological phenomena (e.g., Ref. [36]), it is thus relevant to study the effects of fluctuations on the behavior of chemical systems, and in particular on the mechanisms of pattern formation.

In this paper, we study a particular cubic autocatalytic reaction-diffusion model subject to external fluctuations (represented by an additive-noise term). This stochastic CARD (SCARD) model has been studied numerically in Refs. [21,22], where it is shown that noise can trigger transitions between different types of patterns. Here, we extend those results by studying the phase diagram of the SCARD model as a function of the noise amplitude.

In addition, we present a theoretical analysis of the SCARD model's phase diagram using the renormalization group. The renormalization group is a very powerful tool that can be used to systematically include the effect of fluctuations in certain physical systems. It has been applied in many areas, including particle physics (e.g., Ref. [37]), critical phenomena (e.g., Ref. [38]), and stochastic differential equations (e.g., Refs. [39,40]). Application of the renormalization group to the SCARD model is presented in Refs. [41–45], where it

is shown that model parameters (such as decay rates and reaction-rate constants) vary with the noise amplitude and the scale of observation. This particular feature enables us to explain (at least qualitatively and sometimes quantitatively) some aspects of the CARD model's phase diagram in the presence of noise.

The paper is organized as follows. We begin with a description of the SCARD model in Sec. II, followed by a brief introduction to the renormalization group and derivation of simple relations that can be used to compare with observables from numerical simulations in Sec. III. Section IV presents the numerical results obtained after integration of the SCARD equations for different values of the noise parameter. We compare the numerical results with the results coming from the renormalization group in Sec. V. Finally, some discussion and conclusions are presented.

II. SIMPLEST SCARD MODEL

The SCARD model considered here is defined by the following set of stochastic nonlinear reaction-diffusion equations [21,22]:[1]

$$\frac{\partial v}{\partial t} = -(F+K)v + \lambda u v^2 + \eta_v(\boldsymbol{x},t) + D_v\nabla^2 v, \tag{1}$$

$$\frac{\partial u}{\partial t} = F(u_0-u) - \lambda u v^2 + \eta_u(\boldsymbol{x},t) + D_u\nabla^2 u, \tag{2}$$

where $u = u(\boldsymbol{x},\, t)$ and $v = v(\boldsymbol{x},\, t)$ are the concentrations of the two leading chemical species, D_u and D_v are the diffusion coefficients for both species, K is the decay rate of species v, λ is the rate constant for the autocatalytic chemical reaction, F is the feeding rate of species u in the system, and $\eta_u(\boldsymbol{x},\, t)$, $\eta_v(\boldsymbol{x},\, t)$ denote additive spacetime-dependent noise terms encoding the effect of environmental fluctuations on the system. Note that the autocatalytic term $\lambda u v^2$ is cubic: this is the minimum nonlinearity needed for such systems to exhibit both Hopf and Turing instabilities [9,22]. Note that the results in Ref. [22] were obtained with a generalization of these model to three equations.

The simulation results presented in Sec. IV are obtained by numerically integrating Eqs. (1) and (2) using an explicit two-level forward in time and centered in space integration scheme with zero-flux boundary conditions and using an integration grid array of 501×501 units with spatial step $\Delta x = 1$ and temporal integration step $\Delta t = 0.1$. For both numerical and calculational purposes, in the following we consider a Gaussian white zero-mean noise:

$$\langle \eta_v(k)\eta_v(k')\rangle = \sigma_v^2\,(2\pi)^4\,\delta^{(4)}(k-k'), \tag{3}$$

$$\langle \eta_u(k)\eta_u(k')\rangle = \sigma_u^2\,(2\pi)^4\,\delta^{(4)}(k-k'), \tag{4}$$

where $\sigma_{u;v}$ are the standard deviations of the noise in our numerical simulations. Without loss of generality, we set $\lambda = 1$ and $u_0 = 1$.

III. RUNNING OF THE MODEL PARAMETERS

The treatment of the SCARD model using the renormalization group is presented in detail in Refs. [41–43]. We recap here the main points relevant for our discussion.

The starting point of our renormalization group treatment is the formal solution of Eqs. (1) and (2) in Fourier space. For example, we have for species v

$$v(k) = G_{vo}(k)\Bigg[\eta_v(k) + \lambda\int\frac{d^2\boldsymbol{k}_1}{(2\pi)^2}\frac{d\omega_1}{(2\pi)}\int\frac{d^2\boldsymbol{k}_2}{(2\pi)^2}\frac{d\omega_2}{(2\pi)}v(k_1) \times\, v(k_2)u(k-k_1-k_2)\Bigg], \tag{5}$$

where we used the shortcut notation $v(k) = v(\boldsymbol{k},\omega)$ and defined the free-response function $G_{vo}(\boldsymbol{k}) = (D_v|\boldsymbol{k}|^2 - i\omega + F + K)^{-1}$. The formal solution (5) is an iterative expansion with an infinite number of terms. If the amplitudes of fluctuations are small (i.e., $\sigma_{u;v}$ are small), then it is reasonable to neglect higher-order terms in the expansion and keep only the first correction term proportional to λ.

Typically, the correction terms in Eq. (5) diverge upon integration. These divergences can be systematically absorbed into the parameters of the model using the tools of renormalization. The result is that the value of parameters vary (or "run") with the scale of observation in the presence of fluctuations (see Ref. [37] for a good discussion of renormalization).

In two dimensions and for white Gaussian noise, only F and K run with scale. The complete derivation of the running of F can be found in Ref. [41] (K is done in a similar way):

$$F(L) = F(L^*) + \frac{\sigma_v^2}{(2\pi)2D_v}\log\left(\frac{L}{L^*}\right) \equiv F(L^*) + \Delta F, \tag{6}$$

$$\begin{aligned} K(L) &= K(L^*) - \frac{\sigma_v^2}{(2\pi)2D_v}\log\left(\frac{L}{L^*}\right) \\ &\quad - \frac{\sigma_v^2}{(2\pi)D_v(K(L^*)+F(L^*))}\log\left(\frac{L}{L^*}\right) \\ &\equiv K(L^*) + \Delta K, \end{aligned} \tag{7}$$

where L is the (spatial) scale of observation and L^* is a reference scale at which parameters $F(L^*)$ and $K(L^*)$ have known measured values. Note that we chose Gaussian white noise for simplicity here, but the present renormalization framework can also be applied to colored (power-law) noise with spatial correlations [41], temporal correlations [53], or both spatial and temporal correlations [42].

The effect of noise on the model parameters induces a renormalization of the parameters, namely the expected behavior of the chemical system under the influence of noise for a given set of parameters is equivalent to the behavior of the

[1] As discussed in Ref. [22], a closely related model was originally considered by Higgins [46] and then by Sel'kov [47] to phenomenologically model some oscillatory properties of extant glycolysis (without diffusion). The Brussels group (Prigogine) developed a very similar model to account for the oscillations in the Belousov-Zhabotinsky chemical reaction [3]. Gray and Scott also considered a similar model in the context of chemical combustion [4,5,48]. These models were homogeneous. Then, the two-species version was extended by Pearson [6] into a reaction-diffusion set of equations which was shown to yield a large variety of spatiotemporal patterns. It was later extended into a stochastic version by Lesmes and collaborators [21].

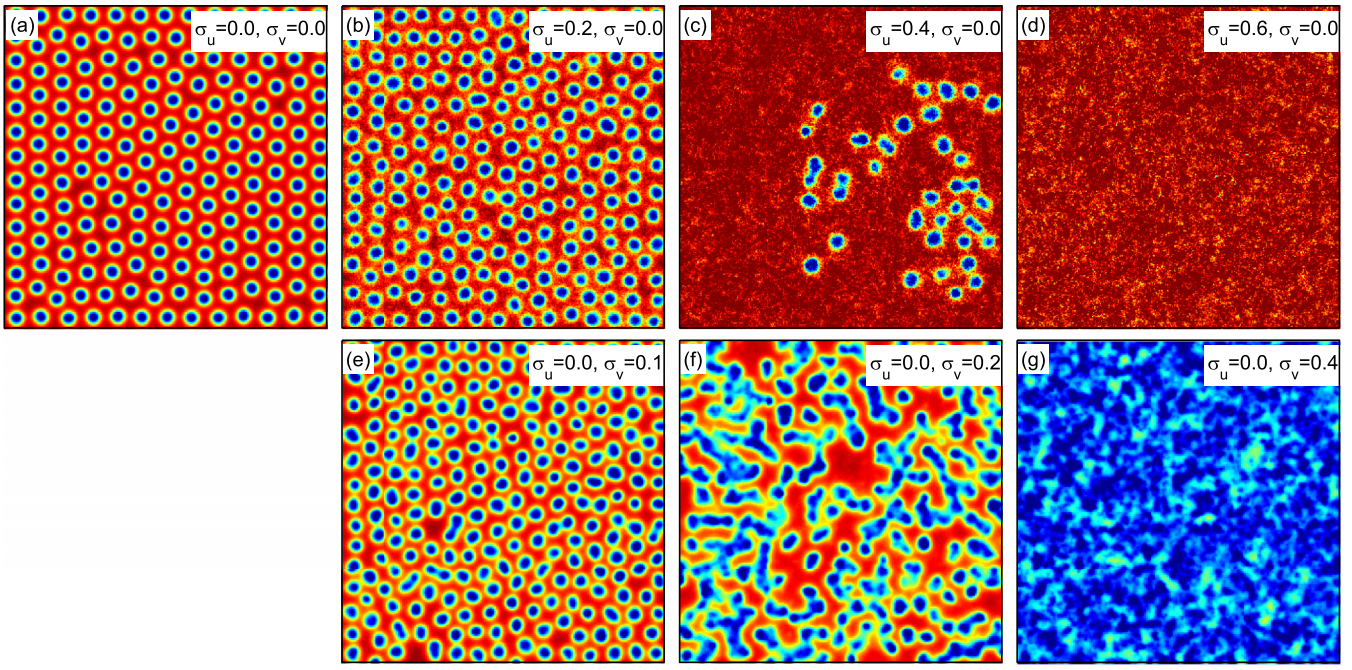

FIG. 1. Effect of noise on both chemical species u and v for a specific pattern. Red (blue) corresponds to a large (small) value of the μ concentration, and a corresponding small (large) value of the v concentration. (a) Pattern that spontaneously appears in the absence of noise for the u variable ($K = 0.0655$, $F = 0.040$, $D_u = 1.0$, $D_v = 0.5$, $\Delta t = 0.1$, and $\Delta x = 1.0$); (b) $\sigma_u = 0.2$ and $\sigma_v = 0.0$; (c) $\sigma_u = 0.4$ and $\sigma_v = 0.0$; (d) $\sigma_u = 0.6$ and $\sigma_v = 0.0$; (e) $\sigma_u = 0.0$ and $\sigma_v = 0.1$; (f) $\sigma_u = 0.0$ and $\sigma_v = 0.2$; and (g) $\sigma_u = 0.0$ and $\sigma_v = 0.4$. (Size of the integrated domain 501×501 px.)

same system without noise with a different set of parameters, with the two sets of parameters connected through Eqs. (6) and (7). Said differently, the change in value of the parameters due to the addition of noise [denoted ΔF and ΔK in Eqs. (6) and (7)] can be exactly "mimicked" by changing the parameters F and K "by hand" by an amount equal to ΔF and ΔK. Expressions (6) and (7) thus provide a road map to follow the evolution of the parameters as the noise amplitude is changed.

Several comments are in order here. First, it is important to emphasize that the formal solution (5) is a perturbative solution only for certain values of the parameters. For the SCARD model, the perturbative expansion is valid when the following criteria are satisfied [41]:

$$\frac{\sigma_v^2}{2D_v F} < 1, \tag{8}$$

$$\frac{\sigma_v^2}{2D_v(K+F)^2} < 1. \tag{9}$$

The above implies that the predictions of perturbation theory and the renormalization group should be interpreted with caution when the noise amplitude σ_v is too large. When those criteria are not satisfied, terms that are higher order in λ in the formal solution (5) must be taken into account. Thus, criteria (8) and (9) determine the regime of validity of perturbation theory.

Second, note that the noise amplitude for the u species, σ_u, does not appear in the running parameter solutions (6) and (7). It can be shown [41] that effects of the η_u noise only appear as second-order corrections in perturbation theory [i.e., corrections proportional to $(\sigma_u^2)^2$]. Since fluctuations are typically small, corrections due to η_u are very small compared to corrections due to η_v. This is consistent with the numerical simulations presented in Fig. 1 and in the Appendix. There, in order to achieve changes in the phase diagram due to η_u comparable to changes due to η_v, values of noise amplitudes at least one order of magnitude larger must be used. For this reason, we do not consider additive noise for species u in the rest of this paper.

IV. NUMERICAL RESULTS

Figure 1 presents the effect of noise for a particular set of parameters. Here, some arbitrarily chosen pattern is considered [Fig. 1(a) without noise] and different noise amplitudes are applied to both u and v variables. The upper row shows the effect of increasing the noise amplitude on the u concentration. Note that the number of domains in the system decreases [Figs. 1(b) and 1(c)] with increasing noise amplitude until they completely disappear, giving rise to a stationary state [red state, Fig. 1(d)]. The lower row presents the effect of noise on the v variable. Again, the configuration of spots is modified [Fig. 1(e)] as the noise amplitude is increased and the system is made to transit into a stripe regime [Fig. 1(f)] and finally a steady state [blue state in this case, Fig. 1(g)]. In this figure, it is possible to observe that the noise amplitude in the system can be used as a parameter to control the final state. Note that much smaller values of the noise in the v variable (lower row in Fig. 1) are needed to achieve the same results as when noise in the u variable is considered (upper row in Fig. 1) in agreement with perturbation theory. From now on, only noise in the v variable will be considered, although equivalent results can be numerically obtained (see

the Appendix) considering noise in the u variable (just higher values of the noise amplitude should be considered). In the following, we numerically consider the effects of fluctuations on the type of structures and their location in the phase diagrams. For simplicity, we consider here that the only source of fluctuations in our model is in the additive term for the v variable (η_v). As argued below Eq. (9), the effects of additive noise in the u variable (η_u) are much smaller than those in the v variable, and can thus be safely neglected. For completeness, we present a sample of simulations with noise in the u variable in the Appendix.

White Gaussian noise with zero mean is considered in all simulations. The only parameters characterizing our fluctuations are the standard deviation σ_v (playing the role of noise amplitude) and the spatial scale L defined as follows in our numerical simulations. Since η_v is space- and time dependent, the minimum resolution for the noise is given by the spatial step Δx ($\Delta x = 1$ in our simulations). We define L as the minimum distance between two different values of noise on the integration grid (which by construction is always a multiple of Δx). The scale L is thus giving information about the coarse graining or "granularity" of the noise considered.

For each value of the noise amplitude σ_v and the scale L, a full F-K phase diagram is calculated. Each phase diagram shows the behavior of the system of Eqs. (1) and (2) for each value of the other model parameters (F and K). Each point in a phase diagram corresponds to at least one simulation of Eqs. (1) and (2). The type of pattern is identified by inspection after letting the simulation reach a steady state. Figure 2 presents a summary of all the simulations performed with noise on the v variable for different values of σ_v and L (keeping $D_u = 2$ and $D_v = 0.7$ fixed). Regions in green correspond to Turing structures (stationary steady structures with a characteristic wavelength determined by the model parameters). Blue regions are related to Hopf solutions (waves, oscillations, etc.). Yellow regions represent solutions of mixed Turing-Hopf modes (corresponding with a co-dimension 2 point in the parameter space). Red regions correspond to values of F and K that produce cell-like behavior [22]. Cell-like behavior (as first named in Ref. [22]) is a specific Turing-Hopf mixed-mode structure with interesting implications for biology [6,22]. Recently [22], they demonstrated that these structures exhibit the same basic properties as simple living organisms in nature. Red and blue dotted regions indicate solutions where the system evolves to a homogeneous red or blue state (large or low value of the u variable).

The lower-left panel in Fig. 2 corresponds to the phase diagram in the absence of noise. A first inspection of the phase diagrams shows that the different regions are completely displaced as the parameters controlling the noise are increased although no new different behavior is observed. In general, all regions are displaced towards the right and top of the phase diagram (larger values of F and K). Focusing on the cell-like region (red region in Fig. 2), one can observe that the domain moves towards the right and top of the phase diagram and increases in size. It implies that this type of behavior becomes more accessible for larger values of noise amplitude. On the other hand, Turing structures (green region) become less accessible and they even disappear in some phase diagrams. This can be understood in the following way: Noise in the system introduces local perturbations on the patterns that become less compatible with the existence of stationary patterns (as it is the case with Turing structures). On the other hand, Hopf or Turing-Hopf regions become larger for the same reason.

V. COMPARISON BETWEEN NUMERICAL AND RENORMALIZATION GROUP RESULTS

In this section, we analyze the information contained in the phase diagrams (cf. Fig. 2) using results coming from the renormalization group [cf. Eqs. (6) and (7)]. In order to do this, it is necessary to find observable properties that can be extracted from simulations and compared with theoretical predictions. We analyze two such properties below: the size of the cell-like region and the characteristic wavelength of structures in the chemical system.

We first analyze the increase in size of the cell-like region due to fluctuations. Renormalization tells us that each point on the phase diagram is displaced when fluctuations are present [cf. Eqs. (6) and (7)]. Imagine a square of size $l = 0.005$ in the deterministic phase diagram (bottom left diagram in Fig. 2). In the presence of noise, this square is distorted into a trapezoid. The area of the trapezoid $A_{trapezoid}$ is given by

$$\begin{aligned} A_{\text{trapezoid}} &= l^2 + l\Delta F\left(\frac{1}{K+F} - \frac{1}{K+F+2l}\right) \\ &= A_{\text{square}} + \Delta A(\sigma_v), \end{aligned} \tag{10}$$

where A_{square} is the area of a square and $\Delta A(\sigma_v)$ is the change in area due to fluctuations. For convenience, we define the following ratio:

$$R = \frac{\Delta A(\sigma_v)}{\Delta A(\sigma_v = 0.075)}. \tag{11}$$

The above ratio characterizes the change in area of an $l \times l$ square due to noise with respect to some arbitrarily chosen reference value, taken to be the change in area when the noise amplitude is $\sigma_v = 0.075$ (i.e., noise amplitude at which perturbation theory is not valid anymore; cf. Eqs. (8) and (9)]. This ratio has the advantage of emphasizing the scaling of the change in area with noise amplitude, and removing any dependence on other variables or artifacts coming from numerical simulations. The ratio R can be computed theoretically using Eqs. (6) and (7), and numerically by measuring the size of cell-like regions on each phase diagram.

Figure 3(a) shows the variation of the ratio R versus the noise amplitude σ_v. The area of the cell-like regions in each phase diagram is measured and the magnitude R calculated for all the values of L considered in our simulations. As predicted, all points lie approximately on the same curve, independently of the value of the noise granularity (for $L > 1$), at least for those values of σ_v compatible with the range of validity of the theory [cf. Eqs. (8) and (9)]. The black vertical dashed line marks the upper limit of the theoretical prediction.

Inspection of Eqs. (6), (7), and (10) shows that the effects of L and σ_v are related. A change in one of the parameters can be compensated by a variation of the other parameter. In other

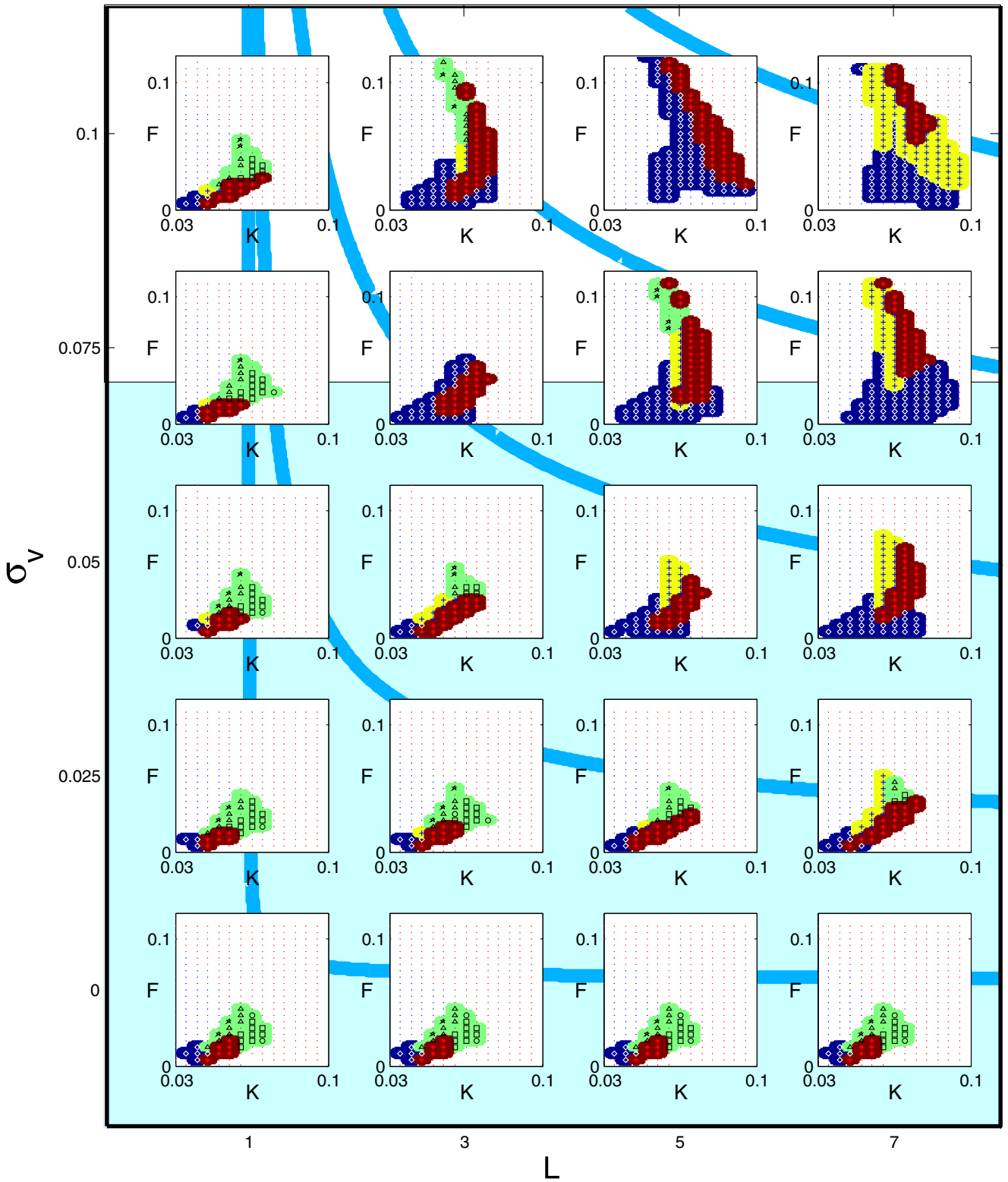

FIG. 2. Effect of fluctuations on the phase diagram of the SCARD model ($D_u = 2.0$ and $D_v = 0.7$). Control parameters here are the noise amplitude (σ_v) and the noise coarse-graining scale (L). Each phase diagram shows the behavior observed for each value of the other model parameters, F and K. Each point in each phase diagram corresponds to at least one simulation of Eqs. (1) and (2). Green regions correspond to Turing structures, blue regions to Hopf solutions (waves, oscillations, etc), yellow regions to Turing-Hopf modes, and red regions to cell-like behavior. Red and blue dotted regions correspond to solutions where the system evolves to a homogeneous red and blue state, respectively. Actual simulations are marked in the diagram with the different points: x = homogeneous steady state, o = Turing spots, • = mix of Turing spots and stripes, Δ = Turing stripes, $\star$ = inverted Turing spots, $\diamondsuit$ = Hopf structures, + = mixed Turing-Hopf modes, and $*$ = cell−like behavior. (501×501 integration domain, $\Delta t = 0.1$, $\Delta x = 1$.)

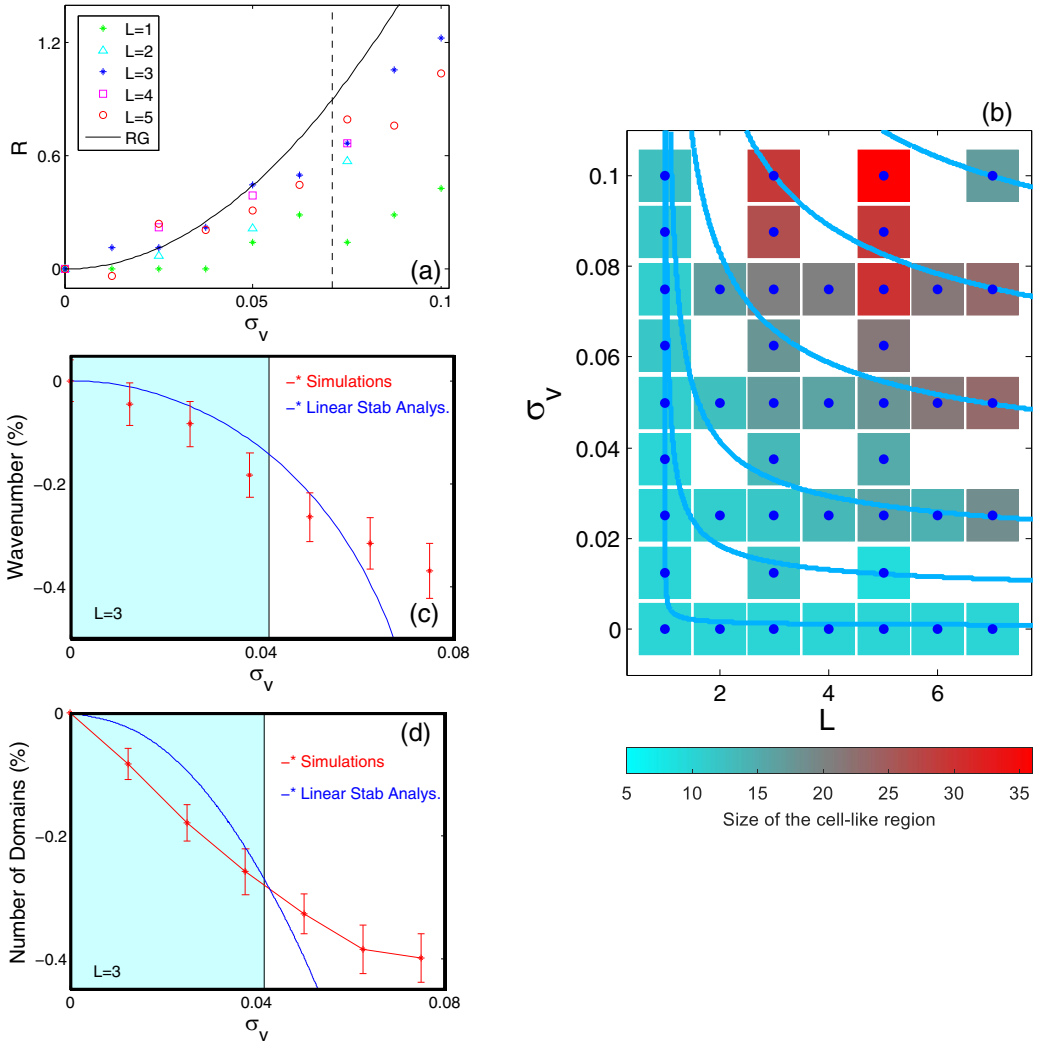

FIG. 3. Comparing renormalization group results with direct numerical simulations of the SCARD model. (a) Variation of R vs σ_v. Solid lines are the renormalization group predictions while points with the different colors and shapes correspond to simulations of the SCARD model for different values of L. (b) Size of the cell-like region in phase diagrams for each value of σ_v and L. Solid lines are renormalization group predictions for regions with similar sizes [cf. Eq. (12)]. (c) Variation of the Turing wave number with σ_v. Blue line is the renormalization group prediction. Red points are calculated directly from the 2D FFT of each simulation. (d) Variation of the number of cell-like domains for a given set of parameters vs σ_v. Blue line is the theoretical prediction and red line corresponds to numerical simulations. Note that perturbation theory is valid only for $\sigma_v < 0.04$.

words, the same phase diagram can be obtained from different sets of (L, σ_v). Focusing on the cell-like region and its size in each of the phase diagrams, we plot (color coded) in Fig. 3(b) the value of the cell-like region size for different values of (L, σ_v): light blue corresponds to the smallest cell-like region size while red corresponds to the largest. Solid blue lines represent the isolines,

$$\frac{\sigma_v^2}{(2\pi)2D_v}\ln\left(\frac{L}{L^*}\right) = \text{const} \tag{12}$$

that are predicted by the renormalization group (the same isolines are also shown in the background of Fig. 2). The trends observed in Fig. 3(b) are consistent with the theoretical predictions.

Turing patterns are also observed in the SCARD model. They are stationary structures characterized by a characteristic wavelength observed by the average distance between each structure. This wave number only depends on the model parameters. Linear stability analysis of Eqs. (1) and (2) can be used to calculate the most probable wave number (or inverse wavelength) of such a pattern [2],

$$k^2_{\text{Turing}} = \frac{D_v f_u + D_u g_v}{2D_u D_v}, \tag{13}$$

where k_{Turing} is the Turing wave number and f_u, f_v, g_u, and g_v are the partial derivatives of the nonlinear functions f and g with respect to u and v variables evaluated at the fixed point (u_o, v_o),

$$f_u = \left.\frac{\partial f(u,v)}{\partial t}\right|_0 = -v_0^2 - F, \tag{14}$$

$$g_v = \left.\frac{\partial g(u,v)}{\partial t}\right|_0 = 2u_0v_0 - (F+K). \tag{15}$$

This wave number depends directly on the model parameters F and K. Thus, according to Eqs. (6) and (7), the Turing wave number (and correspondingly the wavelength) should vary in the presence of fluctuations. We plot in Fig. 3(c) the change in the Turing wave number as a function of the noise amplitude, and compare it to the characteristic wave number directly measured from numerical simulations using fast Fourier transform (FFT). The 2D FFT of each simulation is converted into a 1D plot by averaging over the radial coordinate; the wave number for the maximum of this plot gives the Turing wave number and the broadness of the peak gives an estimate of the error. Note that renormalization group predictions are in good agreement with the numerical results in the parameter region where perturbation theory is valid (region marked in light blue in the figure).

The value of the Turing wavelength can be used to infer the approximate number of Turing spots that actually fit in an integration domain given that size. Since k_{Turing} runs in the presence of fluctuations, it implies that the number of Turing spots should also be affected by noise. Figure 3(d) presents a comparison between the number of domains measured in simulations and the number of domains estimated from k_{Turing} for different values of the noise amplitude σ_v. Note that renormalization group predictions qualitatively reproduce the results from numerical simulations within the limits of validity of perturbation theory (region marked in light blue in the figure).

VI. DISCUSSION AND CONCLUSIONS

The extensive numerical analysis of the SCARD model (1) and (2) done in this paper demonstrates that the effect of fluctuations plays an important role in determining the final state the system may adopt. It extends the results of Refs. [21,22] by systematically analyzing and categorizing all possible final states of the stochastic CARD model. Some of the patterns exhibited might be interesting for biologically inspired research.

From a theoretical point of view, it is known that fluctuations affect the behavior of many systems, and their effects can be analyzed using renormalization techniques. Based on the results of Refs. [41–43], we show how fluctuations can be incorporated into a rescaling of the model parameters. This running of the parameters leads to changes in the phase diagram that are equivalent to a constant change in the model parameters as described by Eqs. (6) and (7). For two observables (size of cell-like regions and Turing wavelength), it is possible to calculate the changes in the phase diagram. Those changes are in qualitative (and to some extent quantitative) agreement with predictions from the renormalization group within the range of validity of perturbation theory, as shown in Fig. 3.

The above shows that noise can be used as a control parameter for a chemical system, triggering noise-induced phase transitions [49,50]. Noise can be used to influence pattern formation (or other behaviors) in a controlled way, and the extent of this influence may be calculated using renormalization techniques in some cases. Our results, thus, open the possibilities of using noise for control of chemical reactions in experimental situations, such as implementing chemical logic gates by dynamically modulating its boundary conditions [51,52] and selecting chemical pathways using additive noise [53].

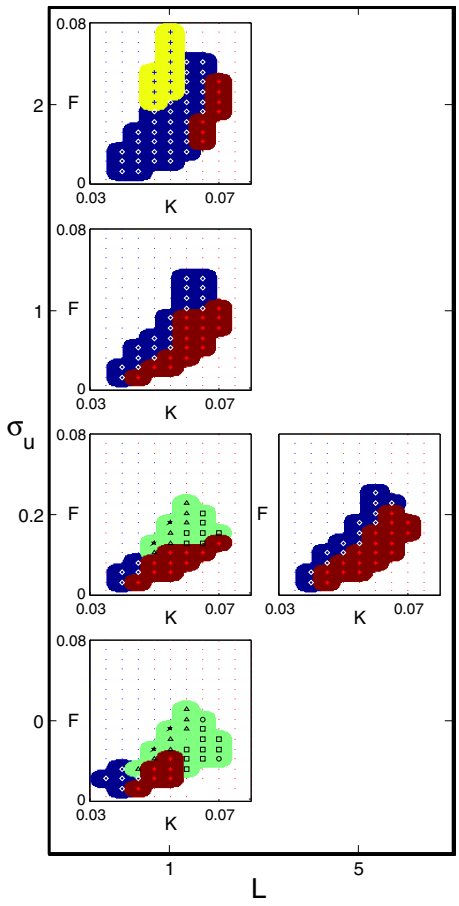

FIG. 4. Effect of fluctuations on the phase diagram for the SCARD model ($D_u = 2.0$ and $D_v = 0.7$). Control parameters here are the noise amplitude on the u variable (σ_u and $\sigma_v = 0$) and the noise coarse graining (L). Each phase diagram shows the behavior observed for each value of the other model parameters, F and K. Each point in each phase diagram corresponds to at least one simulation of Eqs. (1) and (2). Same color coding as in Fig. 2.

ACKNOWLEDGMENTS

We thank Repsol S. A. for supporting this research. The funders had no role in study design, data collection and analysis, decision to publish, or preparation of the manuscript. We also thank Alec Pawling for assistance with the numerical simulations.

APPENDIX: RESULTS ON NOISE FOR SPECIES U

We present in this appendix numerical simulations of Eqs. (1) and (2) considering noise only on the u variable (i.e., we take $\sigma_u \neq 0$ and $\sigma_v = 0$). Results are shown in Fig. 4. Different phase diagrams are presented for different values of the noise parameters. The left column keeps the value of $L = 1$ constant and changes the value of σ_u. The panel on the right presents the influence of L on the phase diagrams for

a constant value of $\sigma_u = 0.2$. Panel in the lower-left corner is the reference without noise. Comparing Fig. 4 with the phase diagrams plotted in Fig. 2, it is possible to note that σ_u must reach much higher values in order to achieve similar effects as those obtained with σ_v. This is in agreement with perturbation theory, which states that effects due to noise in the u concentration appear at higher order compared to noise in the v concentration.

[1] J. D. Murray, *Mathematical Biology I: An Introduction* (Springer, New York, 2002).
[2] J. D. Murray, *Mathematical Biology II: Spatial Models and Biomedical Applications* (Springer, New York, 2003).
[3] G. Nicolis and I. Prigogine, *Self-Organization in Non-Equilibrium Systems* (Wiley, New York, 1977).
[4] P. Gray and S. K. Scott, Chem. Eng. Sci. **39**, 1087 (1984).
[5] P. Gray and S. K. Scott, J. Phys. Chem. **89**, 22 (1985).
[6] J. E. Pearson, Science **261**, 189 (1993).
[7] A. M. Turing, Philos. Trans. R. Soc. **237**, 37 (1952).
[8] V. Castets, E. Dulos, J. Boissonade, and P. DeKepper, Phys. Rev. Lett. **64**, 2953 (1990).
[9] I. R. Epstein and J. A. Pojman, *An Introduction to Nonlinear Chemical Dynamics* (Oxford University Press, New York, 1998).
[10] M. A. Allessie, F. I. M. Bonke, and F. J. G. Schopman, Circ. Res. **33**, 54 (1973).
[11] M. H. Cohen and A. Robertson, J. Theor. Biol. **31**, 119 (1971).
[12] A. N. Zaikin and A. M. Zhabotinsky, Nature (London) **225**, 535 (1970).
[13] B. Hoop and C.-K. Peng, J. Membr. Biol. **177**, 177 (2000).
[14] J. M. A. Carnall, C. A. Waudby, A. M. Belenguer, M. C. A. Stuart, J. J. P. Peyralans, and S. Otto, Science **327**, 1502 (2010).
[15] D. S. A. Simakov and J. Pérez-Mercader, J. Phys. Chem. A **117**, 13999 (2013).
[16] D. S. A. Simakov and J. Pérez-Mercader, Sci. Rep. **3**, 2404 (2013).
[17] A. P. Muñuzuri and J. Pérez-Mercader, J. Phys. Chem. A **121**, 1855 (2017).
[18] J. García-Ojalvo and L. Schimansky-Geier, Europhys. Lett. **47**, 298 (1999).
[19] T. Butler and N. Goldenfeld, Phys. Rev. E **84**, 011112 (2011).
[20] T. Biancalani, F. Jafarpour, and N. Goldenfeld, Phys. Rev. Lett. **118**, 018101 (2017).
[21] F. Lesmes, D. Hochberg, F. Morán, and J. Pérez-Mercader, Phys. Rev. Lett. **91**, 238301 (2003).
[22] A. P. Muñuzuri and J. Pérez-Mercader, Phys. Life Rev. **41**, 64 (2022).
[23] A. Munteanu and R. V. Solé, Int. J. Bifurc. Chaos **16**, 3679 (2006).
[24] H. Wang, Z. Fu, X. Xu, and Q. Ouyang, J. Phys. Chem. **111**, 1265 (2007).
[25] I. Bashkirtseva and A. Pankratov, Math. Methods Appl. Sci. **45**, 8142 (2022).
[26] T. Biancalani, D. Fanelli, and F. Di Patti, Phys. Rev. E **81**, 046215 (2010).
[27] H. Wang, K. Zhang, and Q. Ouyang, Phys. Rev. E **74**, 036210 (2006).
[28] A. P. Kolinichenko and L. B. Ryashko, in *Mathematical Analysis with Applications*, edited by S. Pinelas, A. Kim, and V. Vlasov (Springer, Cham, 2020), p. 195.
[29] I. Sendiña-Nadal, S. Alonso, V. Pérez-Muñuzuri, M. Gómez-Gesteira, V. Pérez-Villar, L. Ramírez-Piscina, J. Casademunt, J. M. Sancho, and F. Sagués, Phys. Rev. Lett. **84**, 2734 (2000).
[30] D. Das and D. S. Ray, Phys. Rev. E **87**, 062924 (2013).
[31] A. Sanz-Anchelergues, A. M. Zhabotinsky, I. R. Epstein, and A. P. Muñuzuri, Phys. Rev. E **63**, 056124 (2001).
[32] G.-Q. Sun, L. Li, Z. Jin, and B.-L. Li, Methods Partial Differ. Equations. **26**, 1168 (2010).
[33] Q. Zheng, Z. Wang, J. Shen, and H. M. A. Iqbal, Adv. Math. Phys. **2017**, 1 (2017).
[34] A. Kolinichenko, I. Bashkirtseva, and L. Ryashko, Mathematics **11**, 451 (2023).
[35] M. F. Adamer, H. A. Harrington, E. A. Gaffney, and T. E. Woolley, Bull. Math. Biol. **82**, 44 (2020).
[36] D. Karig, K. M. Martini, T. Lu, N. A. DeLateur, N. Goldenfeld, and R. Weiss, Proc. Natl. Acad. Sci. USA **115**, 6572 (2018).
[37] M. E. Peskin and D. V. Schroeder, *An Introduction to Quantum Field Theory* (Perseus Books Publishing, Reading, 1995).
[38] J. Zinn-Justin, *Quantum Field Theory and Critical Phenomena* (Oxford University Press, Oxford, 2002).
[39] E. Medina, T. Hwa, M. Kardar, and Y. C. Zhang, Phys. Rev. A **39**, 3053 (1989).
[40] U. C. Taüber, M. Howard, and B. P. Vollmayr-Lee, J. Phys. A: Math. Gen. **38**, R79 (2005).
[41] J.-S. Gagnon, D. Hochberg, and J. Pérez-Mercader, Phys. Rev. E **92**, 042114 (2015).
[42] J.-S. Gagnon, D. Hochberg, and J. Pérez-Mercader, Phys. Rev. E **95**, 032106 (2017).
[43] J.-S. Gagnon and J. Pérez-Mercader, Physica A **480**, 51 (2017).
[44] D. Hochberg, F. Lesmes, F. Morán, and J. Pérez-Mercader, Phys. Rev. E **68**, 066114 (2003).
[45] M. P. Zorzano, D. Hochberg, and F. Morán, Physica A **334**, 67 (2004).
[46] J. Higgins, Proc. Natl. Acad. Sci. **51**, 989 (1964).
[47] E. E. Sel'kov, Eur. J. Biochem. **4**, 79 (1968).
[48] P. Gray and S. K. Scott, Chem. Eng. Sci **38**, 29 (1983).
[49] J. Garcia-Ojalvo and J. M. Sancho, *Noise in Spatially Extended Systems* (Springer, New York, 1999).
[50] W. Horsthemke and R. Lefever, *Noise-Induced Transitions* (Springer, Berlin, 2006).
[51] M. Egbert, J.-S. Gagnon, and J. Pérez-Mercader, J. R. Soc. Interface **15**, 20180169 (2018).
[52] M. Egbert, J.-S. Gagnon, and J. Pérez-Mercader, J. R. Soc. Interface **16**, 20190190 (2019).
[53] J.-S. Gagnon, D. Hochberg, and J. Pérez-Mercader, Phys. Rev. E **98**, 062216 (2018).